Optimal Multi-Sensor Collision Avoidance System for Small Fixed-Wing UAV

Marta Portugal
marta.portugal@tecnico.ulisboa.pt

Instituto Superior Técnico, Universidade de Lisboa, Lisboa, Portugal

November 2023

Abstract

This work provides a solution for the safety enhancement of small fixed-wing UAVs regarding obstacle detection during flight. The main goal is to implement an optimal multi-sensor system configuration. Therefore, preceding works regarding the integration of available sensors in such systems were studied. As a result, select sensors were modeled for collision detection and avoidance simulations using the potential fields method. An optimization study using a genetic algorithm was conducted to find the sets of sensors and respective orientation that result in the best collision avoidance performance. To do so, a set of collision scenarios with both stationary and moving obstacles were randomly generated. This study resulted in relatively simple detection configurations that provided high collision avoidance success rate. The ultrasonic sensor revealed to be inappropriate given its short range, while the laser rangefinder benefited from long range but had very limited field-of-view. In contrast, both the LIDAR and the RADAR are the most promising, as they exhibit a significant range and a broad field-of-view. The best multi-sensor configurations were either a front-facing LIDAR or RADAR, complimented by a pair of laser rangefinders pointing sideways at 10 or 63 degrees, respectively. The assembly of the final system, including sensors and a PixHawk flight controller, was then designed and executed. The appropriate software (PX4, QGroundControl) was also built and adapted to the current work. To validate the proposed system, all sensors were first individually tested. The bench tests attested the accuracy of the sensor specifications and previous simulations. Ground tests on a rover using a simple obstacle avoidance algorithm displayed satisfactory results.
Keywords: Obstacle detection, collision avoidance, sensor fusion, proximity sensors, optimization.

1. Introduction

Unmanned Aerial Vehicles (UAVs) have been receiving considerable attention in a myriad of operations due to their enhanced stability and endurance. However, collision avoidance remains a significant challenge regarding UAV navigation [1].

Drones have been required to exhibit a practical resolution for a Sense and Avoid (S&A) feature as part of the NextGen [2] strategy for integrating UAVs into the U.S. National Airspace System (NAS). In fact, all UAVs must deploy an automated S&A system that provides safety levels comparable to or even superior to those of manned aircraft.

Fittingly, this work addresses the safety enhancement of small fixed-wing UAVs (maximum take-off weight < 25 kg, range < 10 km, endurance < 2 h and flight altitude < 120 m), particularly with regard to obstacle detection during flight and the automatically triggered collision avoidance maneuver. It is part of a comprehensive system that represents a two-stage "sense" and "avoid" problem, being this work focused on the former.

The generic S&A architecture is depicted in Fig. 1. The purpose of the system is to feed updated flight trajectory information to the flight controller so that the UAV can continue to navigate safely. It all starts with the sensing system.

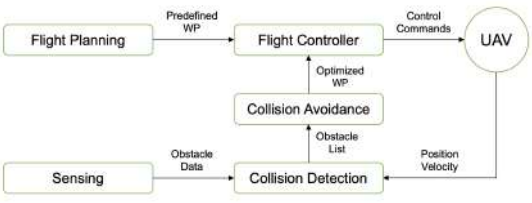

Figure 1: Sense and avoidance architecture.

Preceding this work, detection systems were simulated using laser rangefinders and Radio Detection and Ranging (RADARs) in different configurations [3]. Through the Potential Fields method and resorting to an optimization algorithm, a possible configuration of the UAV sensing system was

reached. Subsequently, ultrasonic sensors and lasers have been employed in the hardware implementation of an effective S&A system on a rover [4].

In this work, the main goal is to leverage insights from the aforementioned studies to implement an adapted and optimized version of said systems onto a rover, as an intermediate step towards generating a robust system for a small fixed-wing UAV.

2. Sensor Modelling

Following are the models of active non-cooperative sensors: the ultrasonic sensor, the laser rangefinder, the LIDAR (Light Detection and Ranging) and the RADAR, as illustrated in Fig. 2; and their comparative analysis in Tab. 1. Some models were developed by [5] and adapted to the present work.

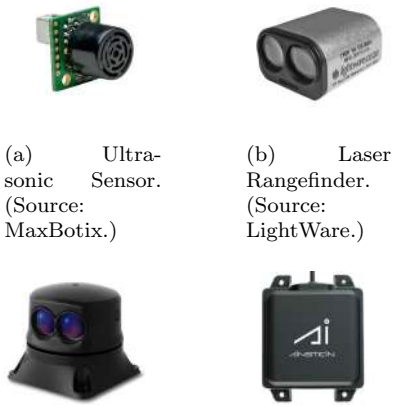

(a) Ultrasonic Sensor. (Source: MaxBotix.)

(b) Laser Rangefinder. (Source: LightWare.)

(c) LIDAR. (Source: LightWare.)

(d) RADAR. (Source: Ainstein.)

Figure 2: Active non-cooperative sensors.

Table 1: Sensor hardware specifications.

	Ultrasonic sensor MB1242 [6]	**Laser rangefinder LW20/C** [7]	**LIDAR SF45/B** [8]	**RADAR US-D1** [9]
Range (m)	7	100	45	50
Horiz. FOV (°)	0	0.3	20-320	43
Resolution (cm)	1	1	1	–
Accuracy (m)	0.1	0.1	0.1	0.04
Update rate (Hz)	7	388	5000	100
Power supply voltage (V)	3-5.5	4.5-5.5	4.5-5.5	5-5.5
Power supply current (mA)	4.4	100	300	400
Outputs & interfaces	Serial & I2C	Serial & I2C	Serial & I2C, Micro USB	UART, CAN
Dimensions (mm)	22x19x15	30x20x43	51x48x44	108x79x20
Weight (g)	5.9	20	59	110
MSRP (€)	40	300	450	600

2.1. Ultrasonic Sensor

This sensor generates a sound, which is then reflected by the obstacle and recorded by the sensor. Thus, the distance from the point of greatest reflection to the obstacle can be calculated. The sonar has a wide FOV that translates to a beam pattern with axial symmetry, as represented in Fig. 3.

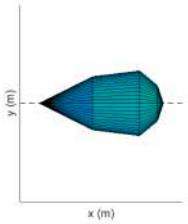

Figure 3: Ultrasonic sensor beam pattern [4].

The model must check for these possibilities at all times:

1. The presence of any spherical surface point within the sonar beam pattern;
2. The perpendicularity of the sound wave direction with its reflecting surface.

Verifying these conditions requires considerable computing time. Therefore, a progressively complex approach was implemented [4]. The closest point to the UAV (among those that passed the filtering) is chosen as the detected point. The UAV reference point, which will serve as the reflection point for the trajectory re-planning algorithm, will be situated on the beam pattern axis at the same distance from the UAV as the detected point.

2.2. Laser Rangefinder

Laser rangefinders are able to compute distances to obstacles by emitting a laser pulse and measuring the time it takes for the reflected beam to be detected, given that laser light beams move at a known speed [10].

Given that all sensors' models may be mounted at an angle β relative to the UAV longitudinal axis, this model assumes the use of two symmetrical sensors at the angles β and $-\beta$ whenever $\beta \neq 0$.

Considering the obstacles as spheres, this can be modeled as a simple interception between a line and a spherical surface given by

$$\|\mathbf{x} - \mathbf{c}\|^2 = r^2 \tag{1a}$$

$$\mathbf{x} = \mathbf{o} + d\hat{\mathbf{u}}\,, \tag{1b}$$

where x is a generic point on the line and/or sphere, c is the centre point of the sphere, r is its radius, $\hat{\mathbf{u}}$ is the unit vector that defines the line direction in $3D$ space and d is the distance from the origin

of the line. Combining both equations leads to an easily solvable quadratic equation,

$$d^2(\hat{\mathbf{u}}\cdot\hat{\mathbf{u}})+2d[\hat{\mathbf{u}}\cdot(\mathbf{o}-\mathbf{c})]+(\mathbf{o}-\mathbf{c})\cdot(\mathbf{o}-\mathbf{c})-r^2=0\,, \quad (2)$$

that returns a solution if $0 < d_{\text{sol}} < \mathbf{R_d}$, where $\mathbf{R_d}$ is the sensor detection range.

2.3. LIDAR

Light Detection and Ranging (LIDAR) emits short and precise laser light impulses with high frequency, that in turn, are reflected and received again by the sensor, measuring the time it took for them to return. Although this technology is similar to the laser rangefinder's, it is multidirectional. Thus, a 3D point cloud can be acquired through an array of distance measurements.

The LIDAR model is very similar to the laser rangefinder's, making only the points that are closest to the sensor detectable. This implies that if an object is totally visible, it is considered that only half is detected and the remaining of the obstacle is reconstructed assuming symmetry, where the center of symmetry is the medium point of the segment connecting the first and last point of the cluster. In the present simulations, this distance corresponds to the diameter of the obstacle.

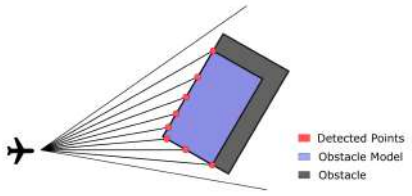

Figure 4: LIDAR obstacle reconstruction [5].

A common issue lies within the higher distance between consecutive points in farther obstacles which results in smaller detected dimensions (see Fig. 4). To solve this problem, the measured diameter is passed through the time filter,

$$D_k = D_{k-1} + G\left(D_{\text{m}} - D_{k-1}\right)\,, \quad (3)$$

where $G(0 < G < 1)$ is the filter gain, D_k is the filtered diameter at instant t_k, D_{k-1} is the filtered diameter at instant t_{k-1}, and D_{m} is the measured dimension at instant t_k. The gain must be carefully chosen because it affects how quickly the dimensions change. While a small gain is better for noisy surroundings, it is not appropriate for objects with high relative speeds. The gain is given by

$$G = 1 - \sqrt[n]{1-p}\,, \quad (4)$$

where p corresponds to a fraction that represents the desired accuracy of the dimensions and n corresponds to the number of filter cycles required to get an accuracy of p. Classic Kalman filters were employed for the tracking phase, where the motion of obstacles was assumed to be two-dimensional, linear, and constant over successive scans.

2.4. RADAR

Radio Detection and Ranging (RADAR) is one of the most popular sensing technologies. It consists of a transmitting antenna producing electromagnetic waves (in the radio or microwave spectrum) and a receiving antenna, which collects waves echoed from obstacles. Despite being very similar to the LIDAR, RADAR technology is distinguished by the frequency of the emitted radiation.

In this case, the state estimation is more complex, given the RADAR sensor provides the range, bearing, and elevation of the observed obstacles. Due to its straightforward implementation, the converted measurement Kalman filter (CMKF) was chosen in [5]. The 2-D model used in the simulations shown is represented by

$$\begin{cases} x_m^u &= \lambda_\alpha^{-1} r_m \cos\left(\alpha_m\right) \\ y_m^u &= \lambda_\alpha^{-1} r_m \sin\left(\alpha_m\right) \end{cases}\,, \quad (5)$$

where (x_m^u, y_m^u) are the measurements converted to the Cartesian frame, r_m is the measured range, α_m is the measured azimuth and λ_α is the bias compensation factor expressed as

$$\lambda_\alpha = e^{-\sigma_\alpha^2/2}\,, \quad (6)$$

where σ_α is the standard deviation of the noise in the azimuth measurements. The compensation of the bias is multiplicative due to the use of the unbiased conversion and modeling the measurement errors as Gaussian white noise. The covariance matrix follows [11].

2.5. Multi-Sensor Data Fusion

All sensor models provide inputs that allow the avoidance system to actuate. However, if the system's architecture is composed by more than one sensor, the data has to be merged. Following best practices [12], the weighted filter method is used in the present study. The principle behind this method is simple: each sensor is given a weight that is based on how reliable it is and the distance measurement for the closest obstacle is computed accordingly, as

$$D_k = \frac{M_k^1 \times W_{M_k^1} + M_k^2 \times W_{M_k^2} + ...M_k^n \times W_{M_k^n}}{W_{M_k^1} + W_{M_k^2} + ...W_{M_k^n}}, \quad (7)$$

where M_k^n is the measurement obtained from sensor n at instant k and $W_{M_k^n}$ is the corresponding weight. To calculate the weights, reference data sensors that provide information about the UAV

state must be installed. A differential norm to compare all conceivable sensor combinations of main data and reference data is applied.

However, the distance output from Eq.(7) is only used if the difference between weights is less than 10%. Otherwise, the obstacle distance measurement corresponding to the sensor with the lowest weight is chosen, and the remaining measurements are discarded on the grounds that they are corrupted.

2.6. Implementation in MATLAB simulation tool

The sensor models were included in a MATLAB simulation that employs the Potential Fields method. To adapt this algorithm to the present work, a comprehensive definition must be established, wherein each detected obstacle is associated with various safety zones. The obstacles can be modeled as spheres, as represented in Fig. 5. The collision radius (R_c) demarks the obstacle's volume, thus, a collision event is registered if the UAV trespasses this radius. The safety radius (R_s) specifies the minimum separation distance between the UAV and the obstacle. When breached, a close call is registered. Finally, the detection radius (R_d) limits the range from which an obstacle is considered by this algorithm.

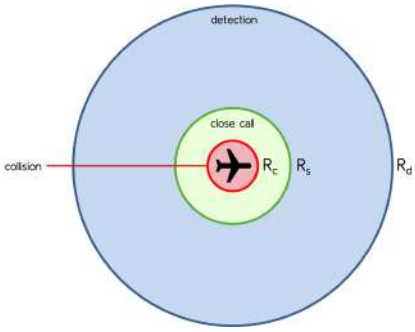

Figure 5: Safety radii for MATLAB simulations.

The Potential Fields method conceptualizes waypoints and obstacles as charged particles. Within this analogy, waypoints create an attractive field, whereas obstacles create a repulsive field and the sum of all forces is used to generate the direction of motion. This allows the simulated UAV to avoid the obstacles' collision and safety radii by replanning its trajectory as it approaches the aforementioned radii.

3. Optimal Sensing System

An optimization study was conducted to find the types of sensors and their orientation relative to the UAV longitudinal axis that result in the best collision avoidance performance. A set of randomly generated collision scenarios with fixed and moving obstacles were generated.

3.1. Scenarios Generation

To create scenarios that are suitable for this study, a scenario generation algorithm was created. Each scenario must specify the obstacle's initial position, velocity and radius. It also includes a pre-planned path and waypoints that the UAV must follow.

Different bounds are defined regarding the kinematic and dimensional properties of the obstacles and the UAV itself. Various stochastic and partially stochastic processes were then extracted from these intervals, creating random values for the different variables.

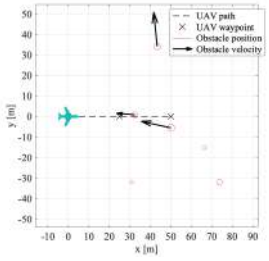

Figure 6: Randomly generated scenario.

An example of a resulting scenario is plotted in Fig. 6. This scenario generating function accepts the predetermined waypoints of the UAV as an input before combining them with a list of moving and static obstacles to produce a scenario. If the UAV does not go beyond any obstacle's safety radius throughout the whole flight simulation (without any sensors), the scenario will be discarded. This function is repeated until n scenarios with an impending collision are generated. For this optimization study, forty collision-leading scenarios were randomly generated, with obstacle parameters varying according to the limits set in Tab. 2.

Table 2: Data for randomly generated imminent collision scenarios.

UAV speed	# fixed obst.	# moving obst.	Obst. radius	Obst. speed	Obst. dir.
[5, 15] m/s	{0, 1, 2}	{0, 1, 2}	[0.5, 2] m	[5, 15] m/s	[0, 90]°

3.2. Optimization Technique and Problem Formulation

To determine the optimal sensor configuration, different sensor sets were tested. The parameters that characterize each sensor model were obtained from their technical manuals or inferred from available data summarized in Tab. 1. Since our simulations were restricted to the horizontal plane of motion, the vertical FOV is not relevant.

In order to optimize the sensor orientation β, a S&A metric function $f(\beta)$, to be minimized, was

defined as

$$f(\beta) = \sum_j \sum_i \Big(-d_{\min}(i) + \phi_1 \left| \max\left(R_s(i) - d_{\min}(i), 0\right) \right|^2 + \\ + \phi_2 \left| \max\left(R_c(i) - d_{\min}(i), 0\right) \right|^2, \tag{8}$$

where the first term drives the evasion maneuver to maximize the minimum distance $d_{\min}$ between the UAV and the obstacle i, the second term represents the penalty when the minimum distance violates the safety radius R_s ($d_{\min} \leq R_s$), and the last term represents the penalty when the minimum distance violates the obstacle collision radius R_c ($d_{\min} \leq R_c$). The metric accumulates not only for every obstacle i in each scenario, but also for all scenarios j. In order to penalize collision cases more than close-calls, the weights were set to $\phi_1 = 10$ and $\phi_2 = 50$.

Since the metric is noisy, the optimization technique selected to find the optimum $f(\beta)$ was the Genetic Algorithm (GA) implemented in MATLAB. The optimization problem can be posed as

$$\begin{aligned} &\text{Minimize } f(\beta) \\ &\quad \text{w.r.t. } \beta \\ &\text{subject to } \beta_{min} \leq \beta \leq \beta_{max} \end{aligned} , \tag{9}$$

where β_{min} and β_{max} are the lower and upper bounds of β, respectively, to be defined for each particular case.

The initial GA population was set to be created with a uniform distribution; the crossover function was set to create 80% of the population in each generation; because the variables are bounded, the mutation function randomly generates directions that are adaptive with respect to the last successful or unsuccessful generation, where the chosen direction and step length satisfy the set bounds. The convergence criteria were set such that the global minimum was found in a timely but accurate manner: a function convergence of 10^{-3} was used with 10 stall generations, and a maximum of 50 generations prescribed. The population size was set to 30 individuals. These parameters were chosen following best practices. The simulations were run on an 1.4 GHz Intel quad-core i5 with 8 GB 2133 MHz RAM.

3.3. Optimal Sensing Configurations

To simplify the problem, the optimization was first carried out for different sets of two sensors with symmetrical orientation about the longitudinal axis, resulting in just one design variable. The orientation of each sensor was bounded between 0° and 90° and each range and FOV was set according to product specifications (see Tab. 1). In the end, the performance of the different sensor sets is summarized in Tab. 3 and compared, in order to implement the best solutions.

3.3.1 Two Ultrasonic Sensors

The results, summarized in the second line of Tab. 3, are far from satisfactory, since the safety radius is breached many times, leading to a collision rate of 10 %. Compared to a single sonar pointing forward (see first line in Tab. 3), a pair of sonars brings little to no gains in detection performance for the type of UAV under study. This was expected due to the short range of ultrasonic sensors, which makes it impossible for the UAV to detect the obstacle, re-plan its trajectory and perform the avoidance maneuver in a timely manner.

3.3.2 Two Laser Rangefinders

The performance of this optimal configuration is summarized in the fourth line of Tab. 3. Although the optimal configuration only fails once in 40 scenarios, the safety radius was breached in 23 of them. This result was expected, since a UAV equipped only with two laser rangefinders (with extremely narrow FOV) is not capable of properly tracking the moving obstacles when collisions are imminent. Also, there are gains when using more than one laser (see third line of Tab. 3).

Compared to the previous case of sonars, these simulations demonstrate that laser rangefinders not only prevent more collisions but also more close calls. This is mainly consequence of their large detection range advantage, that prevail over their almost zero FOV.

3.3.3 Two RADARs

One of the configurations worth studying is a sensor orientation close to 21.5°, which would yield the same result as if the UAV were equipped with a single RADAR with double FOV (86°). Tab. 3 includes the comparison among a single RADAR pointing forward and the solutions with two RADARs in the seventh to eighth lines.

Regarding actual collisions, obstacles that approach the UAV from an angle are more likely to be detected by the optimal solution rather than by the single RADAR configuration. As it can be seen in Tab. 3, the number of failures increase as the orientation decreases (for this particular case), which in turn makes the success rate decrease.

By overlapping the FOV of the two sensors, the accuracy is reduced through the data fusion algorithm. Thus, in this case, having a narrower FOV ($\beta = 9.2°$) and in turn, the juxtaposition of both RADARs, proved to be almost as effective as the double FOV configuration ($\beta = 21.5°$).

These simulations showed that the reduced accuracy of the RADAR proves to be impactful on the precision of obstacle tracking compared to that of

the laser sensors. Despite having a broader FOV and less close calls, the RADAR solution led to just as many collisions, which means that the two laser configuration remains as promising.

3.3.4 Two LIDARs

The SF45/B FOV can range from 20° to 320° (see Tab. 1), thus, a FOV of 180° was chosen. This value ensures a reasonable trade-off between timely scanning frequency and a broad scope.

However, this makes optimization redundant due to the nature of the scenario generation algorithm used. The overlapping of the FOV in the case of a two LIDAR solution does not prove to be advantageous either (note that this is only verified for a FOV of 180°). In this particular case, it is fair to state that the most beneficial solution would be to use a single LIDAR pointing forward, since it decreases hardware cost.

The last line of Tab. 3 includes the performance of this single LIDAR configuration. Compared to the previous types of sensors studied, the LIDAR performs better overall. The reasonable detection range and the wide FOV reduces the chances of close calls and eliminates the possibility of failure.

3.3.5 Performance Comparison of Sensor Sets

Other solutions that involved three sensors were optimized, for example, including two laser rangefinders symmetrical about the UAV longitudinal axis and one fixed RADAR pointing forward. This configuration was also replicated with two lasers and one LIDAR, two RADARs and one laser, and two RADARs and one LIDAR. The performance of the optimal version of these sets of sensors is also summarized in Tab. 3.

Table 3: Comparison of the optimal performance for the different sensor sets studied.

Sensors	Metric	Failure	Close call	Success rate
1 SONAR @ 0 °	1203.8	4/40	32/40	87.5%
2 SONARs @ 36.5 °	804.0	4/40	30/40	90.0%
1 laser @ 0 °	111.1	2/40	28/40	95.0%
2 lasers @ 34.4 °	-414.0	1/40	23/40	97.5%
2 lasers @ 63.4 ° + 1 RADAR @ 0 °	-1240.4	0/40	11/40	100.0%
2 lasers @ 10.0 ° + 1 LIDAR @ 0 °	-1606.4	0/40	8/40	100.0%
1 RADAR @ 0 °	-312.3	4/40	13/40	90.0%
2 RADARs @ 9.2 °	-1171.0	1/40	12/40	97.5%
2 RADARs @ 21.5 °	-1141.7	1/40	12/40	97.5%
2 RADARs @ 35.3 ° + 1 laser @ 0 °	-1480.1	0/40	9/40	100.0%
2 RADARs @ 28.1 ° + 1 LIDAR @ 0 °	-1574.3	0/40	9/40	100.0%
1 LIDAR @ 0 °	-1480.1	0/40	9/40	100.0%

For the set of scenarios tested, the RADAR performed better than the laser, which in turn performed better than the sonar if only one sensor type is to be used. Nonetheless, this is tightly dependent on the sensor characteristics, such as range, FOV and accuracy. Furthermore, a single LIDAR was enough to outperform all other sensors.

All solutions that present a 100% success rate include a RADAR or a LIDAR in their configuration. If the LIDAR is kept out, it is the two RADAR and one laser rangefinder solution that produced the least collisions and led to the least close calls. From these findings, it is expected that increasing the number of sensors even more would lead to better performance, thought at a higher hardware cost.

Comparing the solutions that include a LIDAR, it is proved that it is not significantly advantageous to pair it with other types of sensors, since it already performs distinctively well on its own. Regardless, the two laser and the two RADAR solution are beneficial due to reducing the likelihood of close calls. Despite the LIDAR having a wide FOV that is not increased by either configuration, the chances of breaching the safety radius decrease because the other sensors provide additional detection capacity. *I.e.,* since the LIDAR sweeps the designated area at a certain frequency, there are time instants when a fraction of the area within the LIDAR FOV is 'unsupervised'. Therefore, it is useful to have another set of sensors that track obstacles approaching from that specific area.

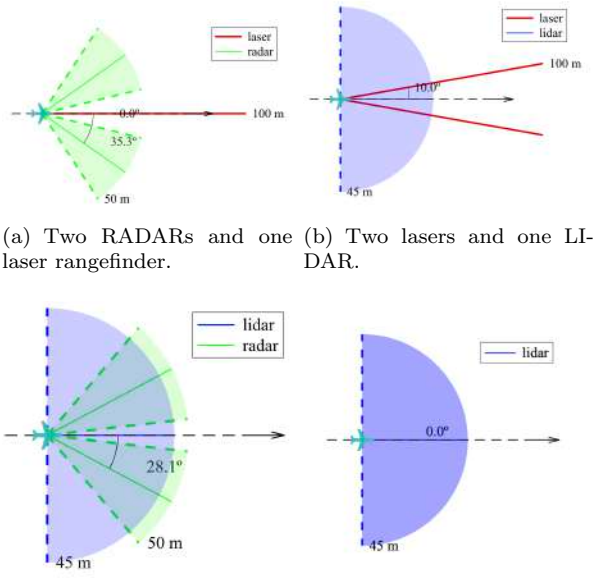

(a) Two RADARs and one laser rangefinder.

(b) Two lasers and one LIDAR.

(c) Two RADARs and one LIDAR.

(d) Single LIDAR.

Figure 7: Highest performance optimal sensor configurations.

To summarize, the optimized configuration had very similar performance in four different cases (reflected in the *Metric* column), being the most promising one composed of one LIDAR pointing forward, complemented by two laser rangefinders pointing at 10° sideways. These four configurations are illustrated in Fig. 7.

4. Hardware and Software Implementation

Some basic concepts are needed to build and fly an unmanned vehicle using PX4. PX4 is a core part of a broader drone platform that includes the QGroundControl ground station, the Pixhawk hardware, and MAVSDK for integration with hardware that uses the MAVLink protocol.

4.1. Flight Controller

PX4 is a powerful open source autopilot flight stack that can be built on a console or in an IDE, for both simulated and hardware targets. PX4 can be run on various hardware platforms, including Pixhawk. The Pixhawk 2.1, or Hex Cube Black, was the chosen controller in [4], so it will also be used in the current work. Generally, the most recent stable released version of PX4 ought to be used, to benefit from bug fixes and get updated features. However, the current stable release (v1.13.3) does not include the driver for the LIDAR used in this work. Consequently, it was necessary to switch to a more recent beta release (v1.14) that includes it. The PX4 source code is stored on a Github repository called PX4/PX4-Autopilot. To get release 1.14 and enable the necessary drivers, the PX4 Developer Guide includes tutorials on Building PX4 Software and PX4 Board Configuration. Once these steps were completed, the PX4 Autopilot firmware could be compiled and uploaded onto the flight controller.

4.2. Ground Control

A ground control station works as a virtual cockpit, serving as an interface between a flight controller and a human operator. Typically, a software running on a computer is connected to the flight controller through wireless telemetry. It can be installed simply by running the executable file available in the QGroundControl online user manual [13].

Once the PX4 firmware is installed onto the flight controller, the user is prompted by QGroundControl to calibrate the vehicle, including the configuration of the controller's built-in sensors, radio receiver, flying modes, power, and motors. Whenever a sensor is connected to the Pixhawk, it must also be activated in QGroundControl.

4.3. Electrical Wiring Layout

The electrical layout could be designed once the hardware is chosen and calibrated. It was possible to connect all the components as shown in Fig. 8 using the connections and supplementary devices (GPS and power module) included in the Cube Black package. The ultrasonic sensor and the laser rangefinder were connected to the I2C ports, whereas the LIDAR and RADAR were connected to TELEM2.

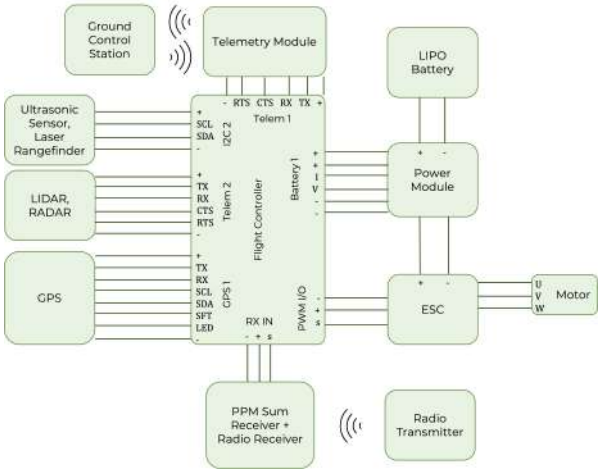

Figure 8: Electrical wiring diagram [4].

5. Bench Tests

Several individual experiments to determine the actual range and FOV restrictions for the chosen devices were performed. These tests included variations in material of the detected obstacle and angles. Figure 9a) demonstrates an experiment where the object to detect is in front of the sensor. In Fig. 9b), the idea was to determine the rangefinder capability of detecting an object which has an angular deflection (θ) in relation to the sensor. During each experiment, a board was positioned at different distances and the sensor data was recorded for 30 seconds for each position.

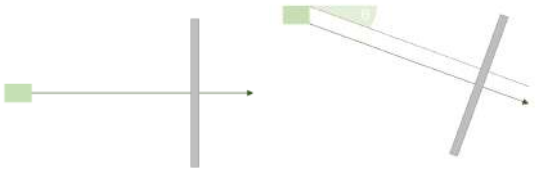

(a) Straight on obstacle. (b) Off-set obstacle.

Figure 9: Sensor bench tests.

5.1. Ultrasonic Sensor

Figure 10a) represents the detection rate of the MB1242 sonar for different materials. When testing with a XPS rather than a wooden board, the maximum range decreased and the sensor performed worse overall. This decrease in performance was

foreseeable since XPS's properties do not match an ideal material (hard, smooth and non-porous).

Figure 10b) shows the MB1242 sonar's detection rate for various distances and orientations. As expected, the sensor performed better when the obstacle was completely in front of it, achieving a maximum range of 435 cm with perfect a detection rate, although the datasheet states 640 cm. Additionally, the maximum range decreased when augmenting θ, which was also an expected behaviour. Moreover, this sensor proved to be very directional as it stopped detecting any targets for $\theta \geq 40°$.

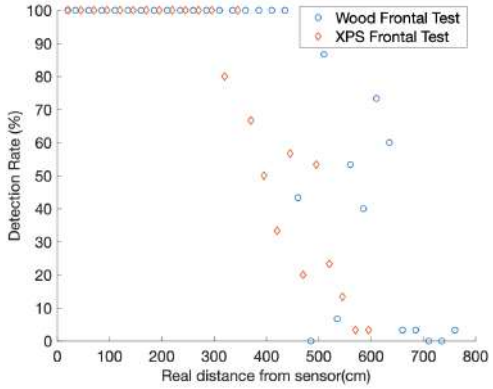

(a) for different materials.

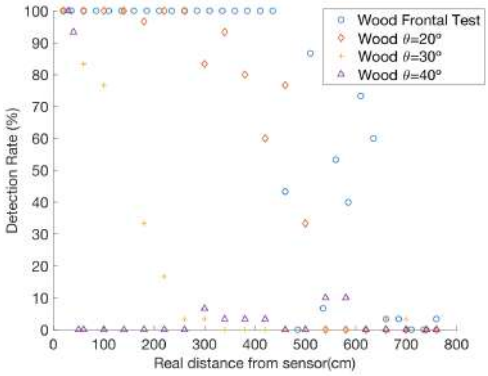

(b) for different angles of incidence.

Figure 10: MaxBotix MB1242 ultrasonic sensor detection rate.

5.2. Laser Rangefinder

In frontal tests, the laser maintained a perfect detection rate before reaching 85 m, as seen in Fig. 11. From this distance onward, the detection rate decreased non-linearly until it reached 100 m (marked as a dashed red line in Fig. 11). Ultimately, the complete range promised in the datasheet was not attained with a perfect detection rate. Since the laser rangefinder is completely directional, it is not necessary to experiment with off-set obstacles.

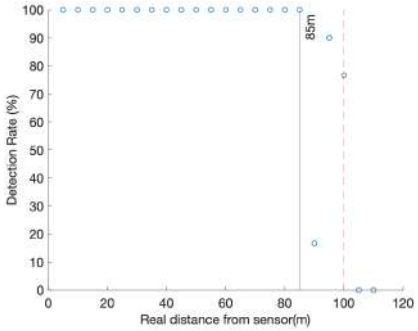

Figure 11: LightWare LW20/C laser rangefinder detection rate (frontal test).

5.3. LIDAR

In the bench tests, the angles of the detected obstacle and scanning speed of the LIDAR were varied. Figure 12 shows the resulting scans from two different experiments: a) the object to detect is in front of the sensor ($\theta = 0$); and b) the object to detect is at 90° in relation to the sensor ($\theta = 90°$).

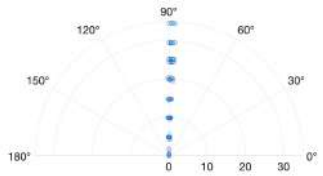

(a) Straight on obstacle.

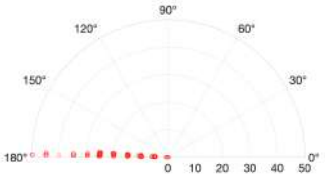

(b) 90° off-set obstacle.

Figure 12: LightWare SF45/B LIDAR bench tests.

As expected, this sensor performed better than the others, maintaining a perfect detection rate through all its range (and for different angles of incidence). However, the average absolute error was overall lower when the obstacle was aligned with the sensor.

Figure 13 illustrates how the length of the arc traversed varies analytically with the distance to the sensor and the angular velocity. This graphic shows that, although the LIDAR has a 50m range, at the maximum scanning speed, it might not be possible to detect an obstacle less than 8m wide at this distance. When the scanning speed is reduced, the sensor is likely to detect a target of at least 2.2 m at maximum distance. At minimum speed, this stops being relevant within the 50 m range.

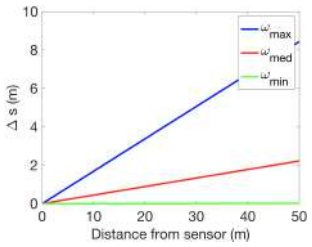

Figure 13: LightWare SF45/B LIDAR undetectable arcs for different scanning speeds.

6. Rover Tests

To be able to implement the most promising detection solutions, the system was tested on a small rover first. Although it is being idealized for a UAV, ground testing the current system was a convenient intermediate step. The experiment consisted of directing the rover along a linear path, equipped with a forward-facing distance sensor, and strategically positioning an obstacle directly in its trajectory, as illustrated in Fig. 14. For these tests, a new eletrical diagram, shown in Fig. 15, and additional software configuration was required.

Figure 14: Rover test.

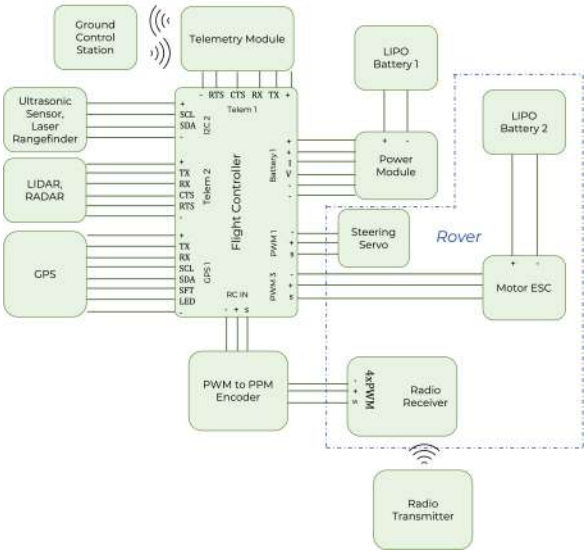

Figure 15: Electrical diagram for rover testing [4].

After placing the rover on a collision path, the avoidance response was extracted and summarized in Fig. 16. The tests were conducted by iterating on the avoidance margin parameter (ranging from 1 to 10 meters in 1m increments), and registering the reported and real distances at which the rover effectively stopped.

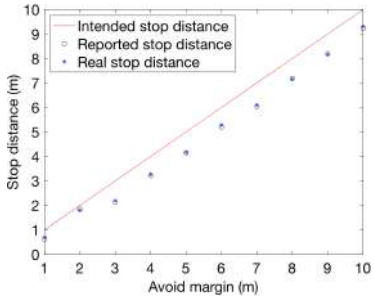

(a) MB1242 sonar.

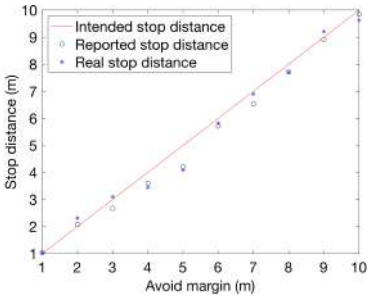

(b) LW20/C laser.

Figure 16: Simple avoidance response with rangefinder mounted on rover.

This process was attempted using an ultrasonic sensor and laser rangefinder. The rover did not always succeed in stopping before the input safety margin, regardless of the sensor in use. However, it performed best with the laser rangefinder, keeping a maximum margin of 80 cm from the intended stop distance. The sonar stop distances were more precise but less accurate, maintaining an average difference of 72 cm from the intended stop distance. Due to the laser's directionality, terrain irregularities were detected before obstacles at times. This behavior highlights the importance of sensor choice. Additional inaccuracies can likely be linked to faulty calibration. Overall, while the avoidance algorithm exhibited satisfactory performance, it offers potential for further refinement to meet the specific needs of this particular application.

7. Conclusions

This work presents a comprehensive solution for enhancing the safety of small fixed-wing UAVs by addressing the critical issue of obstacle detection during flight. A set of select sensors, namely the ultrasonic sensor, laser rangefinder, LIDAR, and RADAR, were identified and further employed in modeling collision detection and avoidance simulations using the potential fields method. Traditional Kalman filters were sufficient to provide

proper tracking for laser rangefinders and LIDARs, but RADARs required a Converted Measurement Kalman Filter with unbiased conversion. Due to its simplicity and efficiency, the weighted filter technique was chosen at the decision level for the data fusion from many redundant sensors.

To determine the best combination of sensors and their orientations, these simulations were used in an optimization study. The study revealed that relatively simple detection configurations can yield a high success rate in collision avoidance. While the ultrasonic sensor is found to be inadequate due to its limited range, the laser rangefinder benefits from a long range, but has a restricted field-of-view. On the other hand, both the LIDAR and RADAR prove to be the most promising options, offering not only a substantial range but also a wide field-of-view. Based on the optimization study, the recommended multi-sensor configurations consist of a front-facing LIDAR or RADAR, accompanied by a pair of laser rangefinders pointing sideways at either 10 °or 63 °.

To validate the proposed system, the necessary hardware and software were implemented, which allowed for the individual testing of each sensor. The bench tests confirmed the accuracy of the sensors specifications and previous simulations. In the case of the ultrasonic sensor, the importance of the material and the angular deflection of the obstacle to be detected was highlighted. As for the laser rangefinder, the key factor proved to be directionality. The LIDAR presented less shortcomings, as expected. However, the sensor's parameters (update rate, angular velocity and scan angle limits) directly affected its performance. More specifically, it is necessary to reach a compromise between the LIDAR scan speed and the effective range of visibility.

A preliminary implementation of the system on a small rover was made. The laser rangefinder consistently performed the best.

This work provides a comprehensive methodology for testing and validation of an optimized multi-sensor system configuration and the proposed system shows great promise for enhancing the safety of small fixed-wing UAVs during flight.

References

[1] Riham Altawy and M. Youssef. Security, privacy, and safety aspects of civilian drones: A survey. *ACM Transactions on Cyber-Physical Systems*, 1(2):1–25, 2016. doi:10.1145/3001836.

[2] Federal Aviation Administration. Next Generation Air Transportation System (NextGen). `https://www.faa.gov/nextgen`, May 2023. Acessed: 13/09/2023.

[3] Nuno Alturas. Modeling and optimization of an obstacle detection system for small UAVs. Master's thesis, Instituto Superior Tcnico, Lisboa, Portugal, January 2021.

[4] Pedro Serrano. Optimization of obstacle detection for small UAVs. Master's thesis, Instituto Superior Tcnico, Lisboa, Portugal, June 2022.

[5] Nuno Alturas and Andr Marta. Modeling and optimization of an obstacle detection system for small fixed-wing UAV. In *Aerobest 2021 - ECCOMAS Thematic Conference on Multidisciplinary Design Optimization of Aerospace Systems*, pages 324–342, Lisboa, Portugal, July 2021. IDMEC. ISBN:978-989-99424-8-6.

[6] MaxBotix. I2CXL-MaxSonar-EZ Datasheet. `https://maxbotix.com/pages/i2cxl-maxsonar-ez-datasheet`, 2021. Acessed: 13/04/2023.

[7] LightWare. Laser rangefinder LW20/C Manual. `https://www.documents.lightware.co.za/LW20%20-%20LiDAR%20Manual%20-%20Rev%2012.pdf`, 2020. Acessed: 13/04/2023.

[8] LightWare. LiDAR SF45/B Guide. `https://support.lightware.co.za/sf45b/#/introduction`, 2021. Acessed: 13/04/2023.

[9] Ainstein. US-D1 Data Sheet. `https://ainstein.ai/wp-content/uploads/US-D1-Data-Sheet.pdf`, 2022. Acessed: 13/04/2023.

[10] Jeffery Saunders, Brandon Call, Andrew Curtis, Randal Beard, and Tim McLain. Static and dynamic obstacle avoidance in miniature air vehicles. In *Infotech@Aerospace*, Arlington, VA, USA, September 2005. AIAA. doi:10.2514/6.2005-6950.

[11] Mo Longbin, Song Xiaoquan, Zhou Yiyu, Sun Zhong Kang, and Y. Bar-Shalom. Unbiased converted measurements for tracking. *IEEE Transactions on Aerospace and Electronic Systems*, 34(3):1023–1027, 1998. doi:10.1109/7.705921.

[12] Nils Gageik, Paul Benz, and Sergio Montenegro. Obstacle detection and collision avoidance for a UAV with complementary low-cost sensors. *IEEE Access*, 3:599–609, 2015. doi:10.1109/ACCESS.2015.2432455.

[13] QGroundControl User Guide. `https://docs.qgroundcontrol.com/master/en/index.html`. Acessed: 25/01/2023.